

Review

Review of the Post-IR IRSL Dating Protocols of K-Feldspar

Junjie Zhang and Sheng-Hua Li *

Department of Earth Sciences, The University of Hong Kong, Hong Kong 999077, China; junjie@connect.hku.hk

* Correspondence: shli@hku.hk

Received: 17 October 2019; Accepted: 10 January 2020; Published: 14 January 2020



Abstract: Compared to quartz, the infrared stimulated luminescence (IRSL) of K-feldspar saturates at higher dose, which has great potential for extending the dating limit. However, dating applications with K-feldspar has been hampered due to anomalous fading of the IRSL signal. The post-IR IRSL (pIRIR) signal of K-feldspar stimulated at a higher temperature after a prior low-temperature IR stimulation has significantly lower fading rate. Different dating protocols have been proposed with the pIRIR signals and successful dating applications have been made. In this study, we review the development of various pIRIR dating protocols, and compare their performance in estimating the equivalent dose (D_e). Standard growth curves (SGCs) of the pIRIR signals of K-feldspar are introduced. Single-grain K-feldspar pIRIR dating is presented and the existing problems are discussed.

Keywords: OSL dating; K-feldspar; post-IR IRSL; standard growth curve (SGC); single-grain

1. Introduction

Optically stimulated luminescence (OSL) dating is applied to date the last exposure event of a mineral grain to sunlight [1]. The OSL ages are obtained by the equation: $\text{Age} = D_e/D_r$, where D_e is the equivalent dose, representing the radiation dose that mineral grains have received after being blocked from sunlight, and the D_r is the environmental dose rate mainly dominated by the radioactive elements U, Th, K. Quartz has long been used as the ideal mineral for OSL dating, because of its abundance in nature, its signal stability, and its susceptibility to bleaching, especially after the single-aliquot regenerative-dose (SAR) protocol was established [2–4]. However, the OSL signal of quartz saturates with relatively low radiation dose, which has limited its application in dating older samples. Studies have shown that the quartz OSL ages were underestimated when the samples were older than ~100 ka [5–7], a situation usually attributed to the early saturation behavior of quartz OSL signal [8]. In some case, such as in the aeolian deposits from the Chinese Loess Plateau, age underestimation began at ~70 ka [9,10], which may be related to abnormally short lifetime of the OSL signal [11,12].

Compared to quartz, the infrared stimulated luminescence (IRSL) of K-feldspar has several advantages: the IRSL signal of K-feldspar saturates at higher dose, which has the potential to date older samples; the IRSL signal intensity of K-feldspar is much greater than quartz OSL signal, providing higher data precision; and the K element within K-feldspar grains provides an internal component for the dose rate, which is not affected by variations of the external environment [13–15]. However, the application of K-feldspar IRSL dating has long been hampered by a phenomenon called anomalous fading [16–18]. The thermally stable luminescence signal of K-feldspar fades under ambient temperature, which is suggested to be a result of quantum tunneling between the electron traps and holes [16–19]. Fading correction method has been proposed to address this problem [14,20,21]. With this solution, the fading rate of IRSL signal for each individual sample needs to be measured, which requires a large amount of laboratory work. In addition, fading correction for older samples

would become more complicated because of the dose-dependent behavior of fading rate [21–24], and age overestimation after fading correction has been widely reported [25–29]. An isochron dating method has also been proposed [30,31]. In this method, it is assumed that the IRSL signal induced by internal dose does not fade, and D_e values of K-feldspar fractions with different grain sizes need to be measured, which is also laborious.

It would be highly advantageous if a non-fading signal of K-feldspar could be identified. Studies that aimed to isolate the non-fading IRSL signals have driven the development of post-IR IRSL (pIRIR) dating protocols, and a detailed review has been published in 2014 [32]. Here, we briefly introduce the pIRIR developments before 2014, and focus on the improvements since 2014.

2. Development of pIRIR Dating Protocols

2.1. Two-Step IR Stimulation

Thomsen et al. [33] found that the IRSL signal stimulated at 225 °C after a preceding IR stimulation at 50 °C (post-IR IRSL) faded much more slowly. The 50 °C IR stimulation (IR_{50}) is supposed to remove the close trap-hole pairs which are prone to tunneling; while the left distant trap-hole pairs stimulated at the subsequent high temperature experience less fading [33–36]. Following the observation of Thomsen et al. [33], Buylaert et al. [37] tested the two-step post-IR IRSL (pIRIR_{50, 225}) dating protocol (Table 1) on K-feldspar extracts from various depositional environments. The fading rate (g_{2days} value) of the pIRIR_{50, 225} signal (mean value, $1.62 \pm 0.06\%/decade$) was significantly lower than the fading rate of the IR_{50} signal (mean value, $3.23 \pm 0.13\%/decade$) [37]. After fading correction, the pIRIR_{50, 225} and IR_{50} signals had similar ages; however, the smaller fading rate made the pIRIR_{50, 225} ages less dependent on the assumptions behind the fading correction model [37].

In order to isolate a more stable pIRIR signal, Thiel et al. [38] increased the temperature of the second-step stimulation from 225 °C to 290 °C (Table 1). The measured fading rate of the pIRIR_{50, 290} signal of loess samples from Austria was 1.0–1.5%/decade, compared to 2.1–3.6%/decade of the IR_{50} signal [38]. However, based on observations that the natural pIRIR_{50, 290} signal of a sample from below the Brunhes/Matuyama geomagnetic reversal boundary was saturated and that a quartz sample also showed a measured fading rate of $1.3 \pm 0.3\%/decade$, Thiel et al. [38] suggested that the fading rate of the pIRIR_{50, 290} signal was a laboratory artifact, and fading uncorrected pIRIR_{50, 290} ages were the most appropriate. Buylaert et al. [39] systematically tested the pIRIR_{50, 290} protocol and concluded that it was a robust dating method for Middle and Late Pleistocene sediments without fading correction.

The pIRIR signals stimulated at higher temperatures (e.g., pIRIR_{50, 225}, pIRIR_{50, 290}, pIRIR_{200, 290}) are more stable than the IR_{50} signal; however, they are also more difficult to bleach [33,37,38]. Thus, the residual doses of the high-temperature pIRIR signals are a concern in dating. Buylaert et al. [40] reported that the residual doses of the pIRIR_{50, 225} and pIRIR_{50, 290} signals from modern aeolian samples of the Chinese Loess Plateau were in the range of 2–8 Gy and 5–19 Gy, respectively. The pIRIR_{50, 290} residual doses of three modern samples from an alluvial bar in Murray et al. [41] were measured to be 5–10 Gy. While quite high pIRIR_{50, 290} residual doses (20–55 Gy) were reported for modern glaciofluvial sediments from a glaciated bay [42]. In various solar bleaching experiments, the measured residual doses of the pIRIR signals varied within a wide range, from less than 2 Gy to >40 Gy [38,39,43–45], and the residual doses increased systematically with higher preheat temperature and stimulation temperature [46–48]. A positive relationship between the residual doses and D_e values has been documented in numerous studies [39,49–54]. With a fixed bleaching time, a linear function between the residual doses and D_e values can be determined, and a minimal residual dose can be obtained by extrapolating to $D_e = 0$ Gy. The minimal residual dose of the pIRIR_{50, 225/290} signal is mostly in the range of 4–7 Gy, which represents the contribution of an un-bleachable component that ubiquitously exists in fully-bleached samples [39,49,50,52–54]. In addition, some studies showed that with extremely long bleaching durations, the residual doses were also reduced to <10 Gy [29,51,52]. In summary, the residual doses of pIRIR₂₉₀ signal for partially-bleached sediments (e.g., glaciofluvial deposits) could be

high (up to ~50 Gy), but the residual doses for well-bleached sediments are, in most cases, smaller than 10 Gy. Some studies argued that bleaching under different natural conditions (e.g., sub-aqueous and sub-aerial) had different efficiency due to different spectrum, which questioned the strategy of residual dose subtraction for D_e measurements [51,55].

For well-bleached old samples, a D_e overestimation of <10 Gy would result in an age overestimation of <~3 ka (e.g., for typical loess sediments), which has small effect. However, it becomes significant for young samples (e.g., of Holocene ages). In order to reduce the effect of residual dose, Reimann et al. [27] proposed a modified two-step pIRIR protocol with the first IR stimulation at 50 °C and the second IR stimulation at 180 °C, together with a preheat temperature of 200 °C (Table 1). The residual dose of the pIRIR_{50,180} signal was reduced to ~1 Gy [27]. Reimann et al. [27] showed that the pIRIR_{50,180} signal was sufficiently stable to date well-bleached middle Holocene and late Pleistocene samples, as the pIRIR_{50,180} ages agreed very well with quartz OSL ages and radiocarbon ages. To make it suitable to date even younger samples (e.g., of hundreds of years), the second IR stimulation was decreased to 150 °C, with a preheat treatment at 180 °C [28,56]. In several studies, the second IR stimulation temperature was changed to 170 °C with the preheat temperature at 200 °C to date Holocene aeolian deposits [57–59].

Table 1. Different pIRIR protocols: pIRIR_{50, 225}; pIRIR_{50, 180}; pIRIR_{50, 290}; pIRIR_{200, 290}; MET-pIRIR; ‘SAR with solar’; ‘MAR with heat’.

Step	pIRIR50,225	pIRIR50, 180	pIRIR50, 290	pIRIR200, 290	MET-pIRIR	‘SAR with Solar’	‘MAR with Heat’
	Buylaert et al. [37]	Reimann et al. [27]	Thiel et al. [38]	Li and Li [60]	Li and Li [26]	Li et al. [61]	Li et al. [62], Modified
1 *	Regenerative dose, D _i						
2	Preheat at 250 °C for 60 s	Preheat at 200 °C for 60 s	Preheat at 320 °C for 60 s	Preheat at 320 °C for 60 s	Preheat at 300 °C for 10 s	Preheat at 300 °C for 60 s	Preheat at 320 °C for 60 s
3	IR for 100 s at 50 °C	IR for 100 s at 50 °C	IR for 200 s at 50 °C	IR for 200 s at 200 °C	IR for 100 s at 50 °C	IR for 100 s at 50 °C	IR for 100 s at 50 °C
4	IR for 100 s at 225 °C	IR for 100 s at 180 °C	IR for 200 s at 290 °C	IR for 200 s at 290 °C	IR for 100 s at 100 °C	IR for 100 s at 100 °C	IR for 100 s at 100 °C
5	Test dose, D _t	IR for 100 s at 150 °C	IR for 100 s at 150 °C	IR for 100 s at 150 °C			
6	Preheat at 250 °C for 60 s	Preheat at 200 °C for 60 s	Preheat at 320 °C for 60 s	Preheat at 320 °C for 60 s	IR for 100 s at 200 °C	IR for 100 s at 200 °C	IR for 100 s at 200 °C
7	IR for 100 s at 50 °C	IR for 100 s at 50 °C	IR for 200 s at 50 °C	IR for 200 s at 200 °C	IR for 100 s at 250 °C	IR for 100 s at 250 °C	IR for 100 s at 250 °C
8	IR for 100 s at 225 °C	IR for 100 s at 180 °C	IR for 200 s at 290 °C	IR for 200 s at 290 °C	Test dose, D _t	Test dose, D _t	IR for 100 s at 300 °C
9	IR at 290 °C for 40 s	Return to step 1	IR at 325 °C for 100 s	IR at 325 °C for 100 s	Preheat at 300 °C for 10 s	Preheat at 300 °C for 60 s	Cutheat to 500 °C
10	Return to step 1		Return to step 1	Return to step 1	IR for 100 s at 50 °C	IR for 100 s at 50 °C	Test dose, D _t
11					IR for 100 s at 100 °C	IR for 100 s at 100 °C	Preheat at 320 °C for 60 s
12					IR for 100 s at 150 °C	IR for 100 s at 150 °C	IR for 100 s at 50 °C
13					IR for 100 s at 200 °C	IR for 100 s at 200 °C	IR for 100 s at 100 °C
14					IR for 100 s at 250 °C	IR for 100 s at 250 °C	IR for 100 s at 150 °C
15					IR at 320 °C for 100 s	Solar simulator for 2 h	IR for 100 s at 200 °C
16					Return to step 1	Return to step 1	IR for 100 s at 250 °C
17							IR for 100 s at 300 °C

* For SAR protocols, in the first cycle, $i = 0$ and $D_0 = 0$, and the natural signal is measured. The sequence is run with several regenerative doses including a zero dose and a repeat dose, to build the growth curve.

2.2. Multi-Step IR Stimulation

Li and Li [26] proposed a multiple-elevated-temperature (MET) pIRIR dating protocol, with five-step IR stimulations from 50 °C to 250 °C with an increment of 50 °C (Table 1). An advantage of this protocol is that there are multiple D_e values corresponding to IR stimulations at different temperatures. Once the D_e reaches a plateau in the high temperature range, it would provide firm evidence that the high-temperature pIRIR signals are sufficiently stable and experience negligible anomalous fading (Figure 1) [26]. Later, the five-step MET-pIRIR protocol was modified to a six-step MET-pIRIR protocol, with the highest IR stimulation temperature increased from 250 °C to 300 °C, and the preheat temperature increased from 300 °C to 320 °C [63]. For the studied loess and desert samples from north China, the fading rates of the IR₅₀ signal were 3–5%/decade, while the fading rates of MET-pIRIR₂₅₀ or MET-pIRIR₃₀₀ signals were very close to zero [26,63].

From the solar bleaching experiments, residual doses of the MET-pIRIR₂₅₀ signal were mostly in the range of 2–10 Gy, although in some cases they were up to ~20 Gy [26,64–68]. In order to make the MET-pIRIR protocol suitable for dating Holocene sediments, Fu and Li. [69] developed a modified low-temperature MET-pIRIR protocol. The preheat temperature was set to 200 °C and the five-step IR stimulation was performed from 50 °C to 170 °C with a step of 30 °C. The residual dose of the MET-pIRIR₁₇₀ signal was generally less than 1 Gy [69]. For Holocene samples, Fu and Li. [69] observed an age plateau between the stimulation temperatures of 110–170 °C. The five-step stimulation can be simplified to a three-step stimulation at temperatures of 110, 140, 170 °C. With the three-step protocol, the age plateau still existed at the stimulation temperatures of 140 °C and 170 °C, indicating that the pIRIR signals at 140 °C and 170 °C can be considered as sufficiently stable over the timescale of Holocene period [69]. Thus, Fu and Li. [69] further simplified the three-step protocol to a two-step protocol, with IR stimulations at 110 °C and 170 °C. Although no age plateau can be observed with the two-step IR stimulation, the pIRIR_{110, 170} signal can still provide identical ages as the five-step pIRIR₁₇₀ signal, the three-step pIRIR₁₇₀ signal, and the quartz OSL signal. However, when the first IR stimulation temperature was decreased from 110 °C to 50 °C, the corresponded pIRIR_{50, 170} ages were slightly underestimated [69].

As pIRIR signals stimulated at higher temperatures are more difficult to be bleached, several studies have proposed that the different bleaching rates of MET-pIRIR signals can be applied to infer the degree of bleaching, and thus to trace the transport history of sediments [70,71].

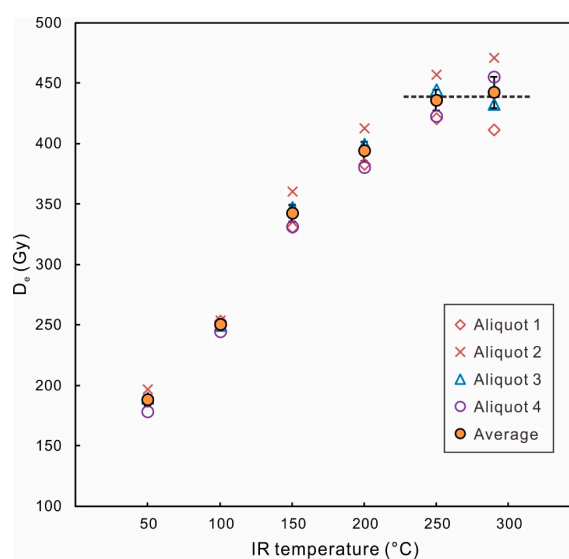


Figure 1. D_e versus IR stimulation temperature in the MET-pIRIR protocol. The sample used is 14LC-11.0, from the top of the L2 layer (second loess layer, corresponding to Marine Isotope Stage 6) in the Luochuan section, Chinese Loess Plateau (Zhang et al. [72]). Four aliquots were measured. The error bar of the average is the standard error calculated from four aliquots.

2.3. Modified Protocols to Extend the Dating Limit

The two-step pIRIR or MET-pIRIR protocols discussed above are all based on the conventional SAR protocol, with a subsequent test dose signal (T_x) to correct for the change in the sensitivity of the regenerative dose signal (L_x). Each aliquot is measured repeatedly with several cycles to build its individual growth curve [8]. The growth curve of the luminescence signal with the radiation dose can be fitted with a single saturating exponential function:

$$I = I_0 + I_{max} * (1 - e^{-D/D_0}), \quad (1)$$

where I is the luminescence signal, D is the radiation dose, and D_0 is called the characteristic saturation dose which quantifies the saturation behavior of the signal.

For quartz, D_0 varies significantly between different grains and samples, but in most cases it is smaller than 200 Gy [73–76]. It is suggested that for reliable dating with quartz, the D_e should not exceed the $2D_0$ limit [8]. Although D_0 of the K-feldspar pIRIR signal varies with different samples and experimental parameters (e.g., test dose, IR stimulation temperature), it is usually around 200–500 Gy with the conventional SAR protocol (Table 2). Applying the $2D_0$ limit, the dating range of the K-feldspar pIRIR signals would not exceed 1000 Gy. To extend the dating limit, modified protocols have been proposed based on the dose-dependent sensitivity of the MET-pIRIR signals from K-feldspar [61,62,77]. Li et al. [62] applied the multiple-aliquot regenerative-dose (MAR) protocol, but added a second test dose (T_2) after a ‘cutheat to 600 °C’ treatment behind the first test dose (T_1). The T_1/T_2 signal was applied to represent the dose-dependent sensitivity. For the MET-pIRIR₂₅₀ signal, the D_0 of the T_1/T_2 signal was ~740 Gy, which was significantly larger than that of the L_x/T_1 signal (~340 Gy). In addition, the L_x/T_2 signal also had a D_0 of ~770 Gy, close to that of the T_1/T_2 signal. Chen et al. [77] presented that with the L_x/T_2 signal, the D_e of a sample from the fifth paleosol layer (S5) of the Chinese loess sequence, corresponding to Marine Isotope Stage (MIS) 13–15, was estimated to be 1360 ± 200 Gy, which was broadly consistent with the expected D_e of 1550 ± 72 Gy. The modified MAR protocol is termed ‘MAR with heat’ in the text below (Table 1). Li et al. [61] modified the conventional SAR protocol, by adding a solar bleaching treatment behind each cycle—‘SAR with solar’ (Table 1). It was found that solar bleaching was able to reset the luminescence sensitivity. Hence, the regenerative dose signal (L_x) or the test dose signal (T_x) can be used alone to estimate the D_e . Here, the T_x is used to represent the dose-dependent sensitivity. While the D_0 of the L_x/T_x signal was ~400 Gy, the D_0 of both the L_x and T_x signals was ~800 Gy [61].

These modified MAR and SAR protocols have greatly increased the D_0 of the K-feldspar pIRIR signal, and have extended the dating limit of K-feldspar to ~1500 Gy. Zhang and Li [78] proposed that a D_0 of ~800 Gy was very likely to be the intrinsic property of the pIRIR signals. In the conventional SAR protocols, the signals of the test dose (D_t) would be overestimated due to the effect of the preceding regenerative dose [43,78–82]. Multiple hypotheses have been proposed to account for the overestimation, such as the thermally transferred signal [43,79], signal inheritance [80,81], and dose dependent sensitivity change [62,82]. The test dose signal following a larger regenerative dose would be overestimated in a higher degree, and the corresponding L_x/T_x would be underestimated more significantly; hence the fitted growth curves have apparently lower D_0 values (200–500 Gy) compared to the intrinsic D_0 (~800 Gy). A larger test dose would reduce such an effect, thus a positive relationship between D_0 and D_t has been observed in numerous studies (Figure 2) [78–81,83,84].

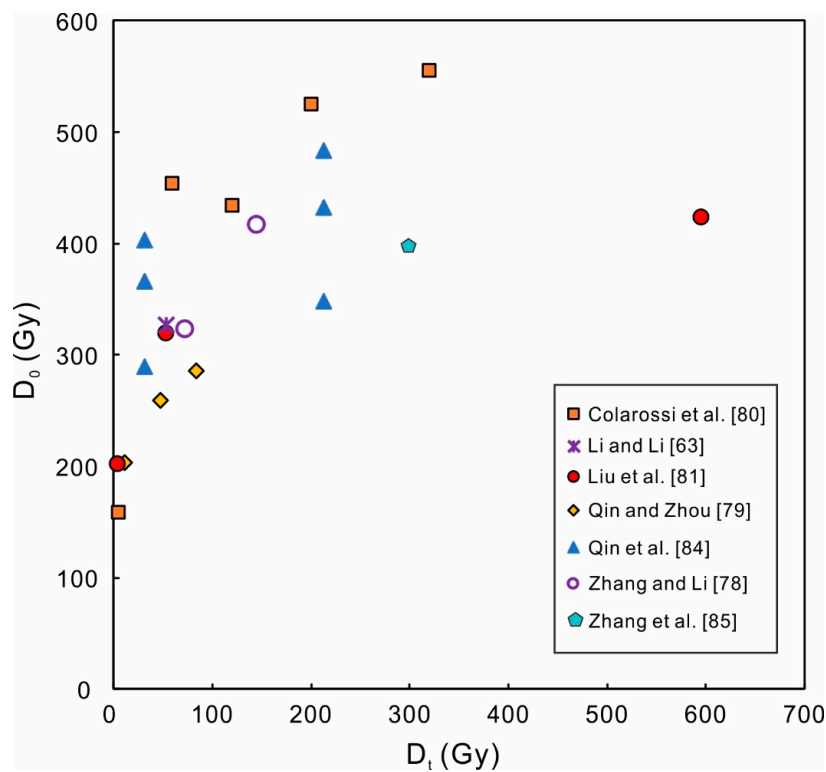


Figure 2. Characteristic saturation dose (D_0) of the pIRIR signals versus the test dose (D_t), with the SAR protocol. Data are from Table 2. A general positive relationship exists between D_0 and D_t . Please note that the pIRIR signals in this graph includes different kinds of signals, such as pIRIR_{50, 170}, pIRIR_{50, 225}, pIRIR_{50, 290}, MET-pIRIR_{250/300} signals. So the D_0 is scattered even with the same D_t .

Table 2. Characteristic saturation dose (D_0) of the growth curves from the conventional SAR protocol with different pIRIR signals.

Signal	D0 (Gy)	Test Dose (Gy)	Reference
pIRIR _{50, 295}	204 ± 5	12	Qin and Zhou [79]
	286 ± 24	84	
pIRIR _{50, 290}	203	4	Liu et al. [81]
	320	53	
	424	595	
pIRIR _{50, 225}	159 ± 87	5	Colarossi et al. [80]
	455	60	
	435	120	
	526	200	
	556 ± 66	320	
pIRIR _{50, 290}	290	32	Qin et al. [84]
	349	213	
pIRIR _{50, 225}	367	32	
	433	213	
pIRIR _{50, 170}	404	32	
	484	213	
MET-pIRIR ₂₅₀	327 ± 16	54	Li and Li [63]
MET-pIRIR ₃₀₀	250 ± 12	54	
MET-pIRIR ₂₅₀	324 ± 5	72.5	Zhang and Li [78]
	417 ± 9	145	
MET-pIRIR ₃₀₀	396 ± 13	300	Zhang et al. [85]

3. Comparison between Different pIRIR Protocols

Several studies have been performed to investigate the pIRIR₂₉₀ D_e dependence on the prior-IR stimulation temperature, and these studies suggested that the D_e values did not change significantly with the prior-IR stimulation temperature varied in the range of 50–260 °C [39,52–54,86]. From a comparison of the D_e values obtained with the pIRIR_{50, 290}, pIRIR_{200, 290}, MET-pIRIR₂₅₀ signals, Li and Li [60] showed that the estimated D_e values were consistent between the three signals when D_e was less than ~400 Gy; however, when the expected D_e exceeded ~400 Gy, the pIRIR_{50, 290} signal had underestimated D_e results compared to the other two signals. Li and Li [60] suggested that the 50 °C prior-IR stimulation was too weak to completely remove the prone-to-fade signal. Qiu and Zhou. [87] compared the performance of four signals, which were pIRIR_{50, 290}, pIRIR_{200, 290}, three-step pIRIR_{200, 290} signal with first stimulation at 50 °C, second stimulation at 200 °C and last stimulation at 290 °C, IRoff-pIRIR_{200, 290} signal with isothermal holding (IR-off) for 200 s before the 290 °C IR stimulation, respectively. The D_e values of their tested samples were within the range of 400–900 Gy. Only the pIRIR_{50, 290} signal had underestimated the D_e values, whereas the other three signals provided consistent D_e results [87]. Buylaert et al. [39] revealed that when the prior-IR stimulation temperature was increased from 50 °C to 200 °C, the intensity of corresponded pIRIR_{200, 290} signal was only 7% of the pIRIR_{50, 290} signal. However, it was later found that the pIRIR₂₉₀ signal intensity was still sufficiently high to guarantee precise measurements even when the prior-IR stimulation temperature was as high as 260 °C, and thus Buylaert et al. [88] applied the pIRIR_{200, 290} protocol to date the last interglacial paleosol (S1) in the Chinese Loess Plateau. Stevens et al. [89] reported that D_e values were underestimated when the prior-IR stimulation temperature was below 140 °C, but a D_e plateau had been reached when the prior-IR stimulation temperature was ≥ 170 °C; and the pIRIR_{200, 290} protocol was adopted to date the Chinese loess back to the S2 layer (second paleosol layer, corresponding to MIS 7). Ito et al. [29] carried out prior-IR stimulation temperature test on marine terrace deposits from Japan, and the results showed that the pIRIR₂₉₀ D_e plateau existed when the prior-IR temperature was within the range of 100–200 °C; while the pIRIR₂₉₀ D_e was underestimated with a prior-IR temperature of 50 °C and overestimated with a prior-IR temperature of 250 °C. A study performed on rock slices showed that the pIRIR₂₉₀ signal from naturally saturated slices was close to the laboratory saturation level only when the first-IR stimulation temperature was high (e.g., 200 °C or 250 °C) [81]. These studies suggest that the first-IR stimulation is better to be performed at a higher temperature (e.g., 200 °C) when dating older samples with the pIRIR₂₉₀ signal.

All of the foregoing comparisons in this section are based on the SAR protocol. However, the upper dating limit of these pIRIR SAR protocols has seldom been studied. A sample from the fifth loess layer (L5) of the Mangshan loess-palaeosol sequence of China was dated to be 401 ± 35 ka with the pIRIR_{200, 290} protocol, which was much younger than the expected age within MIS 12 [87]. Zhang et al. [85] showed that with the SAR protocols, irrespective of the pIRIR_{200, 290} signal or the MET-pIRIR_{250/300} signal, the D_e values were underestimated when the expected D_e exceeded ~800 Gy, whereas the 'MAR with heat' protocol could provide reliable D_e estimates. The SAR D_e underestimation began to occur at the D_e value of ~800 Gy, which was close to twice the D_0 (~400 Gy with SAR protocol) for samples in Zhang et al. [85]. This indicates that the empirical $2D_0$ limit is also applicable to D_e measurements with K-feldspar.

Figure 3A shows that for a loess sample with the D_e of ~640 Gy, the SAR D_e values are smaller compared to the MAR D_e values for the low-temperature signals, but they become similar for the high-temperature (250 °C and 300 °C) signals. Several studies have illustrated that sensitivity correction in the first cycle (natural signal measurement) of the SAR protocol is unsuccessful for the low-temperature IRSL signals (e.g., IR₅₀) of K-feldspar when a high preheat temperature (e.g., >200 °C) is applied, and D_e underestimation exists for those low-temperature signals [67,84,90–92]. Age underestimation of the low-temperature IRSL signals has two sources with the SAR protocol—the anomalous fading and the failure of sensitivity correction. Some studies proposed that the failure of sensitivity correction was related to the increased electron trapping probability caused by the

first preheat treatment [67,90,91]; while a recent study suggested that it was a combined effect of the decrease in the electron trapping probability and the increase in recombination probability [84]. The sensitivity correction of the high-temperature pIRIR signals is generally acceptable [67,84,91,92], which is why consistent SAR D_e and MAR D_e values can be obtained at the temperatures of 250 °C and 300 °C for relatively young samples (Figure 3A). However, the SAR D_e value becomes smaller than the MAR D_e value for a sample with D_e of ~900 Gy (Figure 3B) [85]. Despite of the generally successful sensitivity correction of the high-temperature pIRIR signals, both slight SAR D_e underestimation or overestimation can still occur, depending on the stimulation temperature of the pIRIR signals, the size of the D_e and the test dose, as well as sample origins [52,67,82,84,89]. Zhang et al. [85] performed dose recovery tests on the samples from their study, and observed a 10% overestimation for the dose recovery ratios with a recovery dose of 900 Gy, which cannot explain the SAR D_e underestimation for these old samples.

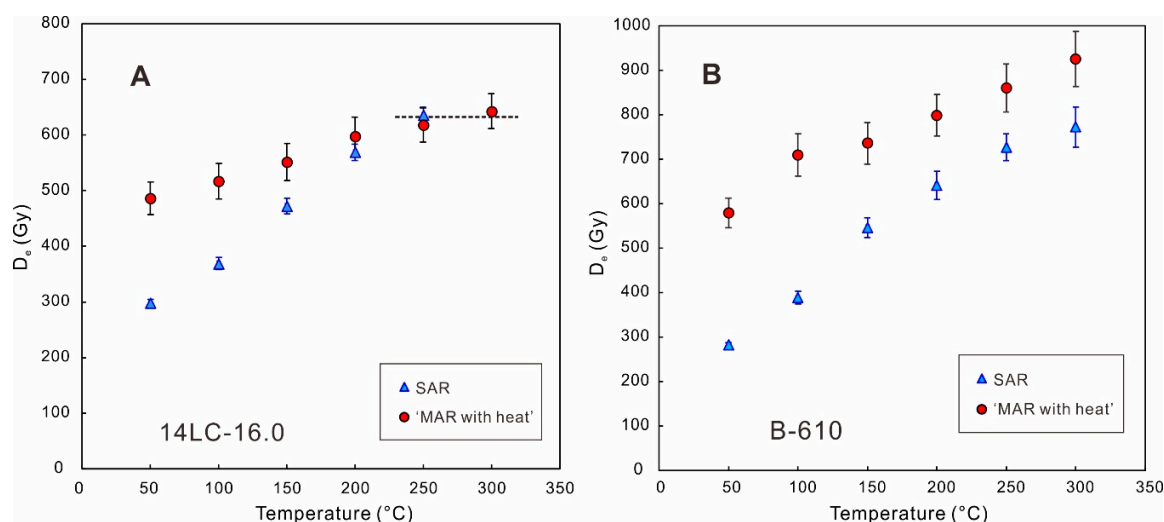


Figure 3. Comparison of D_e values obtained by the conventional SAR protocol (Li and Li [63]) and the modified ‘MAR with heat’ protocol (Li et al. [62]), with a six-step IR stimulation from 50 °C to 300 °C. (A) Sample 14LC-16.0 is from the base of the L2 layer (second loess layer, MIS 6) in the Luochuan section, Chinese Loess Plateau. The higher degree of SAR D_e underestimation compared to MAR D_e at low IR stimulation temperatures is due to the failure of sensitivity correction. Note that the D_e values are still consistent between the SAR and MAR protocols at higher IR stimulation temperatures (250 °C and 300 °C). (B) Sample B-610 is from the Jingbian section of Chinese Loess Plateau. Note that the SAR D_e values are still underestimated at high IR stimulation temperatures compared to the MAR D_e values, because D_e is already larger than 800 Gy. Figure 3B is modified from Zhang et al. [85].

The empirical $2D_0$ limit was initially proposed for quartz [8]. A recent study argued that the D_e underestimation beyond the $2D_0$ limit of quartz was caused by the rejection of the ‘saturated’ aliquots or grains which resulted in a truncated D_e distribution [93]. Instead of the conventional ‘mean D_e ’ method, Li et al. [93] proposed a ‘mean L_n/T_n ’ method to overcome this problem. The ‘mean L_n/T_n ’ method applies the mean of re-normalized natural signal (L_n/T_n) to calculate the final D_e , thus no grains or aliquots would be abandoned when their natural signals lie above the saturation level of the growth curve. This method has been successfully applied in dating quartz of archeological cave sediments with D_e values up to ~300 Gy [94]. However, for the K-feldspar samples whose SAR D_e values were underestimated in Zhang et al. [85], no ‘saturated’ aliquots were observed and discarded. Applying the ‘mean L_n/T_n ’ method cannot overcome the D_e underestimation of K-feldspar in Zhang et al. [85]. Several studies revealed that the natural dose response curve of quartz saturated at lower dose than the laboratory dose response curve, and they suggested it was the reason for quartz D_e underestimation in

the high dose range [74,95–97]. Whether the natural dose response curve of K-feldspar also saturates at lower dose than the laboratory dose response curve needs further research.

4. Standard Growth Curves

The standard growth curve (SGC) was initially proposed for quartz to simplify the measurement procedure of D_e estimation [98]. Test dose standardized OSL signal ($L_x/T_x \times D_t$) was applied to construct the SGC [98]. With the SGC, only the sensitivity corrected natural signal (L_n/T_n) needs to be measured to estimate the D_e , which has greatly improved the efficiency of OSL dating [98]. However, some studies reported that if different D_t values were used, the $L_x/T_x \times D_t$ signal were still deviated from each other, with larger $L_x/T_x \times D_t$ for larger D_t [99,100]. Later, a regenerative dose normalization (re-normalization) procedure was proposed [101,102]. For each individual aliquot, the sensitivity corrected signals (L_x/T_x) are firstly re-normalized by a signal (L_{r1}/T_{r1}) from the aliquot itself. The re-normalized signal (I) is obtained by the following equation:

$$I = \frac{L_x/T_x}{L_{r1}/T_{r1}}, \quad (2)$$

where L_x/T_x are the sensitivity corrected signals of all the regenerative doses and L_{r1}/T_{r1} is the sensitivity corrected signal of a specific regenerative dose (D_{r1}). The I values of different aliquots and samples are plotted together, against the regenerative doses, to fit the SGC with appropriate functions such as the single saturating exponential (SSE) function, double saturating exponential (DSE) function, and general-order kinetic (GOK) function [103]. To estimate D_e , two cycles of the conventional SAR protocol need to be performed. The first cycle is to measure the natural signal (L_n/T_n) and the second cycle to measure the signal (L_c/T_c) of a regenerative dose, which is here termed the calibration dose (D_c). It is better to use a D_c that is close to the expected D_e value [78,102,104]. The L_c/T_c is used to calibrate the L_n/T_n :

$$f(D_e) = f(D_c) \frac{L_n/T_n}{L_c/T_c}, \quad (3)$$

where the $f(D_c)$ is the corresponded functional value of D_c on the SGC. The SGC D_e can be estimated from the $f(D_e)$ according to the SGC function.

The D_t applied in the SGC construction of K-feldspar was 24–66 Gy in Li et al. [102]. Due to the small size of the test dose, no dependence had been observed between the shape of the SGC and the D_t [102]. Zhang and Li [78] applied two larger D_t (72.5 Gy, 145 Gy) for SGC constructions, and reported that the SGC with a D_t of 145 Gy had a larger D_0 than the SGC with a D_t of 72.5 Gy. As illustrated above, D_0 generally increases with D_t (Figure 2). Zhang and Li [78] suggested that the D_t used for SGC D_e estimation should be close to the D_t used for SGC construction. Identical D_t for SGC construction and D_e estimation would always be the best choice.

A least-squares normalization procedure ('LS-normalization') was proposed to establish the SGCs for quartz from Haua Fteah cave, Libya [76]. Later, this LS-normalization procedure has also been applied in constructing SGCs for K-feldspar [92,105]. The 'LS-normalization' can further reduce the inter-grain and inter-aliquot variation of individual growth curves. It involves an iterative re-scaling and fitting process [76]. First, a starting curve is chosen. Then, individual growth curve of each aliquot or grain is re-scaled by multiplying a factor to make the sum of squared residuals—the difference between the observed values and the fitted values—is the smallest. All the rescaled-data are fitted again with a certain function. Iterate the re-scaling and fitting process until there is negligible change (<1%) in the results. The procedure can now be easily performed with the lsNORM function in the R package 'numOSL' [106].

For quartz, different grains or aliquots have quite different D_0 values, and different SGCs need to be built for quartz groups with different saturation behaviors [76,94]. In Figure 2, the D_0 values of K-feldspar are scattered even when the D_t is similar. That is because the figure includes different kinds of pIRIR signals (pIRIR_{50, 170}, pIRIR_{50, 225}, pIRIR_{50, 290}, MET-pIRIR₂₅₀, etc.). Also, the maximum

regenerative doses used to build the growth curves in different studies are also different. Usually, the D_0 would increase when the maximum regenerative dose is larger [107]. When using the same D_t , the identical pIRIR signal from K-feldspar has quite similar saturation behavior between different samples [78,102,105]. Individual growth curves of different K-feldspar grains or aliquots from different continents become very close to each other after re-normalization or re-scaling, which indicates the existence of a global SGC of K-feldspar [102,105].

With a SGC, the machine time needs to estimate the D_e is only 1/3 of the time with a standard SAR approach, but the D_e values obtained by the SGC method are almost identical to the SAR D_e values [78,102]. Similar to quartz, the SGC also provides the 'mean L_n/T_n ' solution to date K-feldspar samples with natural signals close to saturation [108], which cannot be accomplished with the conventional SAR approach.

5. Single-Grain Dating

The conventionally used aliquots in OSL dating usually contain hundreds of grains. The D_e values determined by aliquots are the mean of multiple grains. For partially-bleached samples, it would result in age overestimation. Single-grain dating measures the D_e values of individual grains, thus it has great advantages in dealing with partially-bleached sediments. By applying certain age models (e.g., [109–113]), the portion of fully-bleached grains can be distinguished and the last exposure event can be dated. Single-grain dating is also applicable to sediments that were well-bleached at deposition, but suffered disturbance after burial which resulted in mixing between different-aged grains (e.g., [114–118]). Several studies have applied single-grain dating of K-feldspar with the low-temperature IRSL signal (e.g., at 50 °C) [119–125]. Different methods were applied to overcome the fading problem, such as the *fadia* method [119–121], the isochron method [122], isolating 'zero'-fading grains [123], and fading correction [124,125]. After the pIRIR dating protocol was established, single-grain pIRIR dating with K-feldspar has been reported in numerous studies [43,108,126–137]. The machine time can be saved by performing prior-IR stimulations on all the grains simultaneously [108,129,137].

However, a general trend has been observed that brighter K-feldspar grains (higher signal sensitivity) yield higher D_e values [108,126,129,130,137]. Reimann et al. [126] applied pIRIR_{50, 180} dating protocol on K-feldspar single grains from southern Baltic Sea coast, NE Germany. A dependence of D_e values on the brightness of individual grains was observed—with higher D_e values for brighter grains, and only the brightest 30% of the K-feldspar grains yielded the mean single-grain pIRIR_{50, 180} ages that agreed with the age control [126]. As Reimann et al. [126] found that the fading rates of grains with different brightness were still close to each other, they suggested that the single-grain D_e dependence on brightness might be due to the different K contents in the grains (dimmer grains may contain less K). Brown et al. [129] performed K-feldspar single-grain pIRIR_{50, 225} dating for alluvial fan deposits in Baja California Sur, Mexico. In their study, the grains with brighter signal were found to have smaller fading rates. Rhodes [130] also reported a positive relationship between the grain brightness and D_e values, when dating individual K-feldspar grains from different locations with the pIRIR_{50, 225} signal. Rhodes [130] proposed an improved separation method to select the K-feldspar grains with density smaller than 2.565 g/cm³—the 'Super-K' grains with higher brightness, rather than the regular K-feldspar fraction (density < 2.58 g/cm³).

Jacobs et al. [108] carried out K-feldspar single-grain pIRIR_{200, 275} dating on sediments of the Denisova Cave in southern Siberia. For more than half of their samples, the weighted mean D_e values increased with a higher 'brightness threshold' of the grains (T_n), and similar pattern was also observed in the dose recovery ratios [108]. To make accurate D_e estimation, Jacobs et al. [108] determined a 'threshold' T_n for each sample, above which a mean D_e 'plateau' could be reached. The measured K contents of 60 individual K-feldspar grains (density < 2.58 g/cm³) from Jacobs et al. [108] were mostly in the range of 12–14%, and no dependence of brightness on the K contents was observed. Guo et al. [137] compared the single-aliquot and single-grain MET-pIRIR₁₇₀ D_e results of K-feldspar samples from the Nihewan Basin, northern China. The mean D_e values of single-grain results were smaller than the those

of the single-aliquot results (single-aliquot D_e was dominated by brighter grains inside the aliquot). Applying the 'brightness threshold' method, the mean single-grain D_e values corresponding to brighter grains became close to the single-aliquot D_e values. Fading rate tests showed that dimmer grains had higher fading rates, and Guo et al. [137] suggested that the discrepancy between the single-grain and single-aliquot D_e values were mainly due to the different fading rates of grains. However, a systematic increase in the fading-corrected D_e values with the 'brightness threshold' still existed and they proposed that brighter grains might still have slightly higher internal K contents than dimmer grains [137]. Guo et al. [137] have not observed a dependence of dose recovery ratios on the grain brightness. All the recovery ratios were close to unity irrespective of grain brightness, indicating that the sensitivity correction of natural signal (the first cycle in SAR protocol) is still successful for both bright and dim grains [137].

These studies presented above indicate that it is a ubiquitous phenomenon that brighter K-feldspar grains have higher D_e estimates, and can provide more reliable ages. By now, at least three factors may contribute to the lower D_e values for dim grains. One is that the dim grains have higher fading rates [129,137]. The second is that dim grains contain less internal K (less than 12–14 %), which corresponds to lower environmental dose rate [126,137]. The third is that sensitivity correction of natural signal is not successful for dim grains [108]. The true reason may be a combination of several factors and may also be sample-dependent. Therefore, in single-grain dating of K-feldspar, it is essential to exclude the dim grains with a 'brightness threshold', as age underestimation would be brought in if all grains are included to calculate the mean D_e value. A suitable 'brightness threshold' might be determined by the relationship between the mean D_e values and the 'brightness threshold'—the 'plateau' method [108,137].

6. Conclusions

The pIRIR signals of K-feldspar can be sufficiently stable to provide accurate age estimations without fading correction. However, care should be taken to choose the suitable pIRIR signal to date samples with different ages. For young samples (e.g., <10 ka), the low-temperature signals (e.g., pIRIR_{50, 180}, MET-pIRIR₁₇₀) can be applied with a low preheat temperature (e.g., 200 °C) to avoid the age overestimation caused by residual doses. For intermediate-aged samples (e.g., 10–110 ka), the pIRIR_{50, 290}, pIRIR_{200, 290}, MET-pIRIR₂₅₀ signals are all suitable. For older samples, with D_e larger than 400 Gy (~110 ka with a typical dose rate of ~3.5 Gy/ka), the pIRIR_{50, 290} would underestimate the D_e values, while the pIRIR_{200, 290}, MET-pIRIR₂₅₀ signals can still provide robust results. The empirical upper dating limit of $2D_0$ is also applicable to K-feldspar. With the modified protocols, such as 'MAR with heat' and 'SAR with solar', the dating limit can be increased to ~1500 Gy due to larger D_0 .

The SGC of K-feldspar can greatly save the machine time needed for D_e measurement, while it provides D_e estimates almost identical to those of the standard SAR procedure. In addition, with the SGC, a 'mean L_n/T_n ' approach for D_e estimation can be performed for samples whose natural signals are close to the saturation level of the growth curve. In single-grain dating of K-feldspar, bright grains usually have higher D_e values than the dim grains. Suitable 'brightness threshold' should be applied to exclude the dim grains to avoid age underestimation.

Author Contributions: Conceptualization, S.-H.L. and J.Z.; methodology, J.Z.; writing—original draft preparation, J.Z.; writing—review and editing, S.-H.L. All authors have read and agreed to the published version of the manuscript.

Funding: This research was founded by the grants to S.-H.L. from the Research Grant Council of the Hong Kong SAR, China (awards 17303014, 17307117).

Acknowledgments: We thank two anonymous reviewers and the editor—J.K. Feathers for their constructive comments.

Conflicts of Interest: The authors declare no conflict of interest. The funders had no role in the design of the study; in the collection, analyses, or interpretation of data; in the writing of the manuscript, or in the decision to publish the results.

References

1. Aitken, M.J. *An Introduction to Optical Dating*; Clarendon Press: Oxford, UK, 1998.
2. Murray, A.S.; Roberts, R.G. Measurement of the equivalent dose in quartz using a regenerative-dose single-aliquot protocol. *Radiat. Meas.* **1998**, *29*, 503–515. [[CrossRef](#)]
3. Murray, A.S.; Wintle, A.G. Luminescence dating of quartz using an improved single-aliquot regenerative-dose protocol. *Radiat. Meas.* **2000**, *32*, 57–73. [[CrossRef](#)]
4. Murray, A.S.; Wintle, A.G. The single aliquot regenerative dose protocol: Potential for improvements in reliability. *Radiat. Meas.* **2003**, *37*, 377–381. [[CrossRef](#)]
5. Murray, A.S.; Funder, S. Optically stimulated luminescence dating of a Danish Eemian coastal marine deposit: A test of accuracy. *Quat. Sci. Rev.* **2003**, *22*, 1177–1183. [[CrossRef](#)]
6. Murray, A.S.; Svendsen, J.I.; Mangerud, J.; Astakhov, V.I. Testing the accuracy of quartz OSL dating using a known-age Eemian site on the river Sula, northern Russia. *Quat. Geochronol.* **2007**, *2*, 102–109. [[CrossRef](#)]
7. Andreucci, S.; Sechi, D.; Buylaert, J.P.; Sanna, L.; Pascucci, V. Post-IR IRSL290 dating of K-rich feldspar sand grains in a wind-dominated system on Sardinia. *Mar. Pet. Geol.* **2017**, *87*, 91–98. [[CrossRef](#)]
8. Wintle, A.G.; Murray, A.S. A review of quartz optically stimulated luminescence characteristics and their relevance in single-aliquot regeneration dating protocols. *Radiat. Meas.* **2006**, *41*, 369–391. [[CrossRef](#)]
9. Lai, Z.P. Chronology and the upper dating limit for loess samples from Luochuan section in the Chinese Loess Plateau using quartz OSL SAR protocol. *J. Asian Earth Sci.* **2010**, *37*, 176–185. [[CrossRef](#)]
10. Buylaert, J.P.; Vandenberghe, D.; Murray, A.S.; Huot, S.; De Corte, F.; Van den Haute, P. Luminescence dating of old (> 70 ka) Chinese loess: A comparison of single-aliquot OSL and IRSL techniques. *Quat. Geochronol.* **2007**, *2*, 9–14. [[CrossRef](#)]
11. Fan, A.C.; Li, S.H.; Li, B. Observation of unstable fast component in OSL of quartz. *Radiat. Meas.* **2011**, *46*, 21–28. [[CrossRef](#)]
12. Lai, Z.P.; Fan, A.C. Examining Quartz Osl Age Underestimation for Loess Samples from Luochuan in the Chinese Loess Plateau. *Geochronometria* **2014**, *41*, 57–64. [[CrossRef](#)]
13. Duller, G.A.T. Behavioural studies of stimulated luminescence from feldspars. *Radiat. Meas.* **1997**, *27*, 663–694. [[CrossRef](#)]
14. Huntley, D.J.; Lamothe, M. Ubiquity of anomalous fading in K-feldspars and the measurement and correction for it in optical dating. *Can. J. Earth Sci.* **2001**, *38*, 1093–1106. [[CrossRef](#)]
15. Li, S.H.; Chen, Y.Y.; Li, B.; Sun, J.M.; Yang, L.R. OSL dating of sediments from deserts in northern China. *Quat. Geochronol.* **2007**, *2*, 23–28. [[CrossRef](#)]
16. Wintle, A.G. Anomalous Fading of Thermoluminescence in Mineral Samples. *Nature* **1973**, *245*, 143–144. [[CrossRef](#)]
17. Spooner, N.A. Optical Dating—Preliminary-Results on the Anomalous Fading of Luminescence from Feldspars. *Quat. Sci. Rev.* **1992**, *11*, 139–145. [[CrossRef](#)]
18. Spooner, N.A. The Anomalous Fading of Infrared-Stimulated Luminescence from Feldspars. *Radiat. Meas.* **1994**, *23*, 625–632. [[CrossRef](#)]
19. Visocekas, R. Tunneling Radiative Recombination in Labradorite—Its Association with Anomalous Fading of Thermo-Luminescence. *Nucl. Tracks Radiat. Meas.* **1985**, *10*, 521–529. [[CrossRef](#)]
20. Lamothe, M.; Auclair, M.; Hamzaoui, C.; Huot, S. Towards a prediction of long-term anomalous fading of feldspar IRSL. *Radiat. Meas.* **2003**, *37*, 493–498. [[CrossRef](#)]
21. Kars, R.H.; Wallinga, J.; Cohen, K.M. A new approach towards anomalous fading correction for feldspar IRSL dating—tests on samples in field saturation. *Radiat. Meas.* **2008**, *43*, 786–790. [[CrossRef](#)]
22. Li, B.; Li, S.-H. Investigations of the dose-dependent anomalous fading rate of feldspar from sediments. *J. Phys. D Appl. Phys.* **2008**, *41*, 225502. [[CrossRef](#)]
23. Morthekai, P.; Jain, M.; Murray, A.S.; Thomsen, K.J.; Botter-Jensen, L. Fading characteristics of martian analogue materials and the applicability of a correction procedure. *Radiat. Meas.* **2008**, *43*, 672–678. [[CrossRef](#)]
24. Wallinga, J.; Bos, A.J.J.; Dorenbos, P.; Murray, A.S.; Schokker, J. A test case for anomalous fading correction in IRSL dating. *Quat. Geochronol.* **2007**, *2*, 216–221. [[CrossRef](#)]
25. Li, G.-Q.; Zhao, H.; Chen, F.-H. Comparison of three K-feldspar luminescence dating methods for Holocene samples. *Geochronometria* **2011**, *38*, 14–22. [[CrossRef](#)]

26. Li, B.; Li, S.-H. Luminescence dating of K-feldspar from sediments: A protocol without anomalous fading correction. *Quat. Geochronol.* **2011**, *6*, 468–479. [[CrossRef](#)]
27. Reimann, T.; Tsukamoto, S.; Naumann, M.; Frechen, M. The potential of using K-rich feldspars for optical dating of young coastal sediments—A test case from Darss-Zingst peninsula (southern Baltic Sea coast). *Quat. Geochronol.* **2011**, *6*, 207–222. [[CrossRef](#)]
28. Madsen, A.T.; Buylaert, J.P.; Murray, A.S. Luminescence Dating of Young Coastal Deposits from New Zealand Using Feldspar. *Geochronometria* **2011**, *38*, 379–390. [[CrossRef](#)]
29. Ito, K.; Tamura, T.; Tsukamoto, S. Post-IR IRSL Dating of K-Feldspar from Last Interglacial Marine Terrace Deposits on the Kamikita Coastal Plain, Northeastern Japan. *Geochronometria* **2017**, *44*, 352–365. [[CrossRef](#)]
30. Li, B.; Li, S.-H.; Wintle, A.G.; Zhao, H. Isochron measurements of naturally irradiated K-feldspar grains. *Radiat. Meas.* **2007**, *42*, 1315–1327. [[CrossRef](#)]
31. Li, B.; Li, S.-H.; Wintle, A.G.; Zhao, H. Isochron dating of sediments using luminescence of K-feldspar grains. *J. Geophys. Res.-Earth Surf.* **2008**, *113*. [[CrossRef](#)]
32. Li, B.; Jacobs, Z.; Roberts, R.G.; Li, S.H. Review and assessment of the potential of post-IR IRSL dating methods to circumvent the problem of anomalous fading in feldspar luminescence. *Geochronometria* **2014**, *41*, 178–201. [[CrossRef](#)]
33. Thomsen, K.J.; Murray, A.S.; Jain, M.; Botter-Jensen, L. Laboratory fading rates of various luminescence signals from feldspar-rich sediment extracts. *Radiat. Meas.* **2008**, *43*, 1474–1486. [[CrossRef](#)]
34. Jain, M.; Ankjaergaard, C. Towards a non-fading signal in feldspar: Insight into charge transport and tunnelling from time-resolved optically stimulated luminescence. *Radiat. Meas.* **2011**, *46*, 292–309. [[CrossRef](#)]
35. Poolton, N.R.J.; Wallinga, J.; Murray, A.S.; Bulur, E.; Botter-Jensen, L. Electrons in feldspar I: On the wavefunction of electrons trapped at simple lattice defects. *Phys. Chem. Miner.* **2002**, *29*, 210–216. [[CrossRef](#)]
36. Poolton, N.R.J.; Ozanyan, K.B.; Wallinga, J.; Murray, A.S.; Botter-Jensen, L. Electrons in feldspar II: A consideration of the influence of conduction band-tail states on luminescence processes. *Phys. Chem. Miner.* **2002**, *29*, 217–225. [[CrossRef](#)]
37. Buylaert, J.P.; Murray, A.S.; Thomsen, K.J.; Jain, M. Testing the potential of an elevated temperature IRSL signal from K-feldspar. *Radiat. Meas.* **2009**, *44*, 560–565. [[CrossRef](#)]
38. Thiel, C.; Buylaert, J.P.; Murray, A.; Terhorst, B.; Hofer, I.; Tsukamoto, S.; Frechen, M. Luminescence dating of the Stratzing loess profile (Austria)—Testing the potential of an elevated temperature post-IR IRSL protocol. *Quat. Int.* **2011**, *234*, 23–31. [[CrossRef](#)]
39. Buylaert, J.P.; Jain, M.; Murray, A.S.; Thomsen, K.J.; Thiel, C.; Sohbati, R. A robust feldspar luminescence dating method for Middle and Late Pleistocene sediments. *Boreas* **2012**, *41*, 435–451. [[CrossRef](#)]
40. Buylaert, J.P.; Thiel, C.; Murray, A.S.; Vandenberghe, D.A.G.; Yi, S.W.; Lu, H.Y. IRSL and Post-IR IRSL Residual Doses Recorded in Modern Dust Samples from the Chinese Loess Plateau. *Geochronometria* **2011**, *38*, 432–440. [[CrossRef](#)]
41. Murray, A.S.; Thomsen, K.J.; Masuda, N.; Buylaert, J.P.; Jain, M. Identifying well-bleached quartz using the different bleaching rates of quartz and feldspar luminescence signals. *Radiat. Meas.* **2012**, *47*, 688–695. [[CrossRef](#)]
42. Alexanderson, H.; Murray, A.S. Luminescence signals from modern sediments in a glaciated bay, NW Svalbard. *Quat. Geochronol.* **2012**, *10*, 250–256. [[CrossRef](#)]
43. Nian, X.M.; Bailey, R.M.; Zhou, L.P. Investigations of the post-IR IRSL protocol applied to single K-feldspar grains from fluvial sediment samples. *Radiat. Meas.* **2012**, *47*, 703–709. [[CrossRef](#)]
44. Stevens, T.; Markovic, S.B.; Zech, M.; Hambach, U.; Sumegi, P. Dust deposition and climate in the Carpathian Basin over an independently dated last glacial-interglacial cycle. *Quat. Sci. Rev.* **2011**, *30*, 662–681. [[CrossRef](#)]
45. Li, Y.; Tsukamoto, S.; Frechen, M.; Gabriel, G. Timing of fluvial sedimentation in the Upper Rhine Graben since the Middle Pleistocene: Constraints from quartz and feldspar luminescence dating. *Boreas* **2018**, *47*, 256–270. [[CrossRef](#)]
46. Zhang, J.R.; Tsukamoto, S.; Nottebaum, V.; Lehmkuhl, F.; Frechen, M. D-e plateau and its implications for post-IR IRSL dating of polymineral fine grains. *Quat. Geochronol.* **2015**, *30*, 147–153. [[CrossRef](#)]
47. Wang, Y.X.; Chen, T.Y.; Chongyi, E.; An, F.Y.; Lai, Z.P.; Zhao, L.; Liu, X.J. Quartz OSL and K-feldspar post-IR IRSL dating of loess in the Huangshui river valley, northeastern Tibetan plateau. *Aeolian Res.* **2018**, *33*, 23–32. [[CrossRef](#)]

48. Roberts, H.M. Testing Post-IR IRSL protocols for minimising fading in feldspars, using Alaskan loess with independent chronological control. *Radiat. Meas.* **2012**, *47*, 716–724. [[CrossRef](#)]
49. Sohbaty, R.; Murray, A.S.; Buylaert, J.P.; Ortuno, M.; Cunha, P.P.; Masana, E. Luminescence dating of Pleistocene alluvial sediments affected by the Alhama de Murcia fault (eastern Betics, Spain)—A comparison between OSL, IRSL and post-IR IRSL ages. *Boreas* **2012**, *41*, 250–262. [[CrossRef](#)]
50. Murray, A.S.; Schmidt, E.D.; Stevens, T.; Buylaert, J.P.; Markovic, S.B.; Tsukamoto, S.; Frechen, M. Dating Middle Pleistocene loess from Stari Slankamen (Vojvodina, Serbia)—Limitations imposed by the saturation behaviour of an elevated temperature IRSL signal. *Catena* **2014**, *117*, 34–42. [[CrossRef](#)]
51. Kars, R.H.; Reimann, T.; Ankjaergaard, C.; Wallinga, J. Bleaching of the post-IR IRSL signal: New insights for feldspar luminescence dating. *Boreas* **2014**, *43*, 780–791. [[CrossRef](#)]
52. Yi, S.W.; Buylaert, J.P.; Murray, A.S.; Lu, H.Y.; Thiel, C.; Zeng, L. A detailed post-IR IRSL dating study of the Niuyangzigou loess site in northeastern China. *Boreas* **2016**, *45*, 644–657. [[CrossRef](#)]
53. Li, G.Q.; Rao, Z.G.; Duan, Y.W.; Xia, D.S.; Wang, L.B.; Madsen, D.B.; Jia, J.; Wei, H.T.; Qiang, M.R.; Chen, J.H.; et al. Paleoenvironmental changes recorded in a luminescence dated loess/paleosol sequence from the Tianshan Mountains, arid central Asia, since the Penultimate Glaciation. *Earth Planet. Sci. Lett.* **2016**, *448*, 1–12. [[CrossRef](#)]
54. Li, G.Q.; Li, F.L.; Jin, M.; She, L.L.; Duan, Y.W.; Madsen, D.; Wang, L.B.; Chen, F. Late Quaternary lake evolution in the Gaxun Nur basin, central Gobi Desert, China, based on quartz OSL and K-feldspar pIRIR dating of paleoshorelines. *J. Quat. Sci.* **2017**, *32*, 347–361. [[CrossRef](#)]
55. Lowick, S.E.; Trauerstein, M.; Preusser, F. Testing the application of post IR-IRSL dating to fine grain waterlain sediments. *Quat. Geochronol.* **2012**, *8*, 33–40. [[CrossRef](#)]
56. Reimann, T.; Tsukamoto, S. Dating the recent past (<500 years) by post-IR IRSL feldspar—Examples from the North Sea and Baltic Sea coast. *Quat. Geochronol.* **2012**, *10*, 180–187.
57. Li, G.Q.; Wen, L.J.; Xia, D.S.; Duan, Y.W.; Rao, Z.G.; Madsen, D.B.; Wei, H.T.; Li, F.L.; Jia, J.; Chen, F.H. Quartz OSL and K-feldspar pIRIR dating of a loess/paleosol sequence from arid central Asia, Tianshan Mountains, NW China. *Quat. Geochronol.* **2015**, *28*, 40–53. [[CrossRef](#)]
58. Wang, L.; Jia, J.; Zhao, H.; Liu, H.; Duan, Y.; Xie, H.; Zhang, D.D.; Chen, F. Optical dating of Holocene paleosol development and climate changes in the Yili Basin, arid central Asia. *Holocene* **2019**, *29*, 1068–1077. [[CrossRef](#)]
59. Buckland, C.E.; Bailey, R.M.; Thomas, D.S.G. Using post-IR IRSL and OSL to date young (<200 years) dryland aeolian dune deposits. *Radiat. Meas.* **2019**, *126*, 106131.
60. Li, B.; Li, S.H. A reply to the comments by Thomsen et al. on “Luminescence dating of K-feldspar from sediments: A protocol without anomalous fading correction”. *Quat. Geochronol.* **2012**, *8*, 49–51. [[CrossRef](#)]
61. Li, B.; Roberts, R.G.; Jacobs, Z.; Li, S.H. A single-aliquot luminescence dating procedure for K-feldspar based on the dose-dependent MET-pIRIR signal sensitivity. *Quat. Geochronol.* **2014**, *20*, 51–64. [[CrossRef](#)]
62. Li, B.; Jacobs, Z.; Roberts, R.G.; Li, S.H. Extending the age limit of luminescence dating using the dose-dependent sensitivity of MET-pIRIR signals from K-feldspar. *Quat. Geochronol.* **2013**, *17*, 55–67. [[CrossRef](#)]
63. Li, B.; Li, S.H. Luminescence dating of Chinese loess beyond 130 ka using the non-fading signal from K-feldspar. *Quat. Geochronol.* **2012**, *10*, 24–31. [[CrossRef](#)]
64. Fu, X.; Li, B.; Li, S.H. Testing a multi-step post-IR IRSL dating method using polymineral fine grains from Chinese loess. *Quat. Geochronol.* **2012**, *10*, 8–15. [[CrossRef](#)]
65. Chen, Y.W.; Li, S.H.; Li, B. Residual doses and sensitivity change of post IR IRSL signals from potassium feldspar under different bleaching conditions. *Geochronometria* **2013**, *40*, 229–238. [[CrossRef](#)]
66. Li, B.; Roberts, R.G.; Jacobs, Z. On the dose dependency of the bleachable and non-bleachable components of IRSL from K-feldspar: Improved procedures for luminescence dating of Quaternary sediments. *Quat. Geochronol.* **2013**, *17*, 1–13. [[CrossRef](#)]
67. Zhang, J.J. Behavior of the electron trapping probability change in IRSL dating of K-feldspar: A dose recovery study. *Quat. Geochronol.* **2018**, *44*, 38–46. [[CrossRef](#)]
68. Rui, X.; Zhang, J.F.; Hou, Y.M.; Yang, Z.M.; Liu, Y.; Zhen, Z.M.; Zhou, L.P. Feldspar multi-elevated-temperature post-IR IRSL dating of the Wulanmulun Paleolithic site and its implication. *Quat. Geochronol.* **2015**, *30*, 438–444. [[CrossRef](#)]

69. Fu, X.; Li, S.-H. A modified multi-elevated-temperature post-IR IRSL protocol for dating Holocene sediments using K-feldspar. *Quat. Geochronol.* **2013**, *17*, 44–54. [[CrossRef](#)]
70. McGuire, C.; Rhodes, E.J. Downstream MET-IRSL single-grain distributions in the Mojave River, southern California: Testing assumptions of a virtual velocity model. *Quat. Geochronol.* **2015**, *30*, 239–244. [[CrossRef](#)]
71. Reimann, T.; Notenboom, P.D.; De Schipper, M.A.; Wallinga, J. Testing for sufficient signal resetting during sediment transport using a polymineral multiple-signal luminescence approach. *Quat. Geochronol.* **2015**, *25*, 26–36. [[CrossRef](#)]
72. Zhang, J.J.; Li, S.H.; Sun, J.M.; Hao, Q.Z. Fake age hiatus in a loess section revealed by OSL dating of calcrete nodules. *J. Asian Earth Sci.* **2018**, *155*, 139–145. [[CrossRef](#)]
73. Gong, Z.J.; Sun, J.M.; Lu, T.Y.; Tian, Z.H. Investigating the optically stimulated luminescence dose saturation behavior for quartz grains from dune sands in China. *Quat. Geochronol.* **2014**, *22*, 137–143. [[CrossRef](#)]
74. Timar-Gabor, A.; Wintle, A.G. On natural and laboratory generated dose response curves for quartz of different grain sizes from Romanian loess. *Quat. Geochronol.* **2013**, *18*, 34–40. [[CrossRef](#)]
75. Duller, G.A.T.; Botter-Jensen, L.; Murray, A.S. Optical dating of single sand-sized grains of quartz: Sources of variability. *Radiat. Meas.* **2000**, *32*, 453–457. [[CrossRef](#)]
76. Li, B.; Jacobs, Z.; Roberts, R.G. Investigation of the applicability of standardised growth curves for OSL dating of quartz from Haua Fteah cave, Libya. *Quat. Geochronol.* **2016**, *35*, 1–15. [[CrossRef](#)]
77. Chen, Y.W.; Li, S.H.; Li, B.; Hao, Q.Z.; Sun, J.M. Maximum age limitation in luminescence dating of Chinese loess using the multiple-aliquot MET-pIRIR signals from K-feldspar. *Quat. Geochronol.* **2015**, *30*, 207–212. [[CrossRef](#)]
78. Zhang, J.; Li, S.-H. Constructions of standardised growth curves (SGCs) for IRSL signals from K-feldspar, plagioclase and polymineral fractions. *Quat. Geochronol.* **2019**, *49*, 8–15. [[CrossRef](#)]
79. Qin, J.T.; Zhou, L.P. Effects of thermally transferred signals in the post-IR IRSL SAR protocol. *Radiat. Meas.* **2012**, *47*, 710–715. [[CrossRef](#)]
80. Colarossi, D.; Duller, G.A.T.; Roberts, H.M. Exploring the behaviour of luminescence signals from feldspars: Implications for the single aliquot regenerative dose protocol. *Radiat. Meas.* **2018**, *109*, 35–44. [[CrossRef](#)]
81. Liu, J.F.; Murray, A.; Sohbati, R.; Jain, M. The effect of test dose and first IR stimulation temperature on post-IR IRSL measurements on rock slices. *Geochronometria* **2016**, *43*, 179–187. [[CrossRef](#)]
82. Fu, X.; Li, S.H.; Li, B. Optical dating of aeolian and fluvial sediments in north Tian Shan range, China: Luminescence characteristics and methodological aspects. *Quat. Geochronol.* **2015**, *30*, 161–167. [[CrossRef](#)]
83. Carr, A.S.; Hay, A.S.; Powell, D.M.; Livingstone, I. Testing post-IR IRSL luminescence dating methods in the southwest Mojave Desert, California, USA. *Quat. Geochronol.* **2019**, *49*, 85–91. [[CrossRef](#)]
84. Qin, J.T.; Chen, J.; Li, Y.T.; Zhou, L.P. Initial sensitivity change of K-feldspar pIRIR signals due to uncompensated decrease in electron trapping probability: Evidence from radiofluorescence measurements. *Radiat. Meas.* **2018**, *120*, 131–136. [[CrossRef](#)]
85. Zhang, J.; Li, S.-H.; Wang, X.; Hao, Q.; Hu, G.; Chen, Y. Comparison of equivalent doses obtained with various post-IR IRSL dating protocols of K-feldspar. *Geochronometria* **2020**, in press.
86. Yi, S.; Buylaert, J.-P.; Murray, A.S.; Thiel, C.; Zeng, L.; Lu, H. High resolution OSL and post-IR IRSL dating of the last interglacial–glacial cycle at the Sanbahuo loess site (northeastern China). *Quat. Geochronol.* **2015**, *30*, 200–206. [[CrossRef](#)]
87. Qiu, F.Y.; Zhou, L.P. A new luminescence chronology for the Mangshan loess-palaeosol sequence on the southern bank of the Yellow River in Henan, central China. *Quat. Geochronol.* **2015**, *30*, 24–33. [[CrossRef](#)]
88. Buylaert, J.-P.; Yeo, E.-Y.; Thiel, C.; Yi, S.; Stevens, T.; Thompson, W.; Frechen, M.; Murray, A.; Lu, H. A detailed post-IR IRSL chronology for the last interglacial soil at the Jingbian loess site (northern China). *Quat. Geochronol.* **2015**, *30*, 194–199. [[CrossRef](#)]
89. Stevens, T.; Buylaert, J.P.; Thiel, C.; Ujvari, G.; Yi, S.; Murray, A.S.; Frechen, M.; Lu, H. Ice-volume-forced erosion of the Chinese Loess Plateau global Quaternary stratotype site. *Nat. Commun.* **2018**, *9*, 983. [[CrossRef](#)]
90. Wallinga, J.; Murray, A.; Duller, G. Underestimation of equivalent dose in single-aliquot optical dating of feldspars caused by preheating. *Radiat. Meas.* **2000**, *32*, 691–695. [[CrossRef](#)]
91. Kars, R.H.; Reimann, T.; Wallinga, J. Are feldspar SAR protocols appropriate for post-IR IRSL dating? *Quat. Geochronol.* **2014**, *22*, 126–136. [[CrossRef](#)]
92. Li, B.; Jacobs, Z.; Roberts, R.G. An improved multiple-aliquot regenerative-dose (MAR) procedure for post-IR IRSL dating of K-feldspar. *Anc. TL* **2017**, *35*, 1–10.

93. Li, B.; Jacobs, Z.; Roberts, R.G.; Galbraith, R.; Peng, J. Variability in quartz OSL signals caused by measurement uncertainties: Problems and solutions. *Quat. Geochronol.* **2017**, *41*, 11–25. [[CrossRef](#)]
94. Hu, Y.; Marwick, B.; Zhang, J.F.; Rui, X.; Hou, Y.M.; Yue, J.P.; Chen, W.R.; Huang, W.W.; Li, B. Late Middle Pleistocene Levallois stone-tool technology in southwest China. *Nature* **2019**, *565*, 82–85. [[CrossRef](#)] [[PubMed](#)]
95. Timar-Gabor, A.; Constantin, D.; Buylaert, J.P.; Jain, M.; Murray, A.S.; Wintle, A.G. Fundamental investigations of natural and laboratory generated SAR dose response curves for quartz OSL in the high dose range. *Radiat. Meas.* **2015**, *81*, 150–156. [[CrossRef](#)]
96. Anechitei-Deacu, V.; Timar-Gabor, A.; Thomsen, K.J.; Buylaert, J.P.; Jain, M.; Bailey, M.; Murray, A.S. Single and multi-grain OSL investigations in the high dose range using coarse quartz. *Radiat. Meas.* **2018**, *120*, 124–130. [[CrossRef](#)]
97. Anechitei-Deacu, V.; Timar-Gabor, A.; Constantin, D.; Trandafir-Antohei, O.; Del Valle, L.; Fornos, J.J.; Gomez-Pujol, L.; Wintle, A.G. Assessing the Maximum Limit of SAR-OSL Dating Using Quartz of Different Grain Sizes. *Geochronometria* **2018**, *45*, 146–159. [[CrossRef](#)]
98. Roberts, H.M.; Duller, G.A.T. Standardised growth curves for optical dating of sediment using multiple-grain aliquots. *Radiat. Meas.* **2004**, *38*, 241–252. [[CrossRef](#)]
99. Burbidge, C.I.; Duller, G.A.T.; Roberts, H.M. De determination for young samples using the standardised OSL response of coarse-grain quartz. *Radiat. Meas.* **2006**, *41*, 278–288. [[CrossRef](#)]
100. Shen, Z.X.; Mauz, B. Estimating the equivalent dose of late Pleistocene fine silt quartz from the Lower Mississippi Valley using a standardized OSL growth curve. *Radiat. Meas.* **2011**, *46*, 649–654. [[CrossRef](#)]
101. Li, B.; Roberts, R.G.; Jacobs, Z.; Li, S.H. Potential of establishing a ‘global standardised growth curve’ (gSGC) for optical dating of quartz from sediments. *Quat. Geochronol.* **2015**, *27*, 94–104. [[CrossRef](#)]
102. Li, B.; Roberts, R.G.; Jacobs, Z.; Li, S.H.; Guo, Y.J. Construction of a ‘global standardised growth curve’ (gSGC) for infrared stimulated luminescence dating of K-feldspar. *Quat. Geochronol.* **2015**, *27*, 119–130. [[CrossRef](#)]
103. Guralnik, B.; Li, B.; Jain, M.; Chen, R.; Paris, R.B.; Murray, A.S.; Li, S.H.; Pagonis, V.; Valla, P.G.; Herman, F. Radiation-induced growth and isothermal decay of infrared-stimulated luminescence from feldspar. *Radiat. Meas.* **2015**, *81*, 224–231. [[CrossRef](#)]
104. Peng, J.; Pagonis, V.; Li, B. On the intrinsic accuracy and precision of the standardised growth curve (SGC) and global-SGC (gSGC) methods for equivalent dose determination: A simulation study. *Radiat. Meas.* **2016**, *94*, 53–64. [[CrossRef](#)]
105. Li, B.; Jacobs, Z.; Roberts, R.G.; Li, S.H. Single-grain dating of potassium-rich feldspar grains: Towards a global standardised growth curve for the post-IR IRSL signal. *Quat. Geochronol.* **2018**, *45*, 23–36. [[CrossRef](#)]
106. Peng, J.; Li, B. Single-aliquot Regenerative-Dose (SAR) and Standardised Growth Curve (SGC) Equivalent Dose Determination in a Batch Model Using the Package ‘numOSL’. *Anc. TL* **2017**, *35*, 32–53.
107. Timar-Gabor, A.; Buylaert, J.P.; Guralnik, B.; Trandafir-Antohei, O.; Constantin, D.; Anechitei-Deacu, V.; Jain, M.; Murray, A.S.; Porat, N.; Hao, Q.; et al. On the importance of grain size in luminescence dating using quartz. *Radiat. Meas.* **2017**, *106*, 464–471. [[CrossRef](#)]
108. Jacobs, Z.; Li, B.; Shunkov, M.V.; Kozlikin, M.B.; Bolikhovskaya, N.S.; Agadjanian, A.K.; Uliyanov, V.A.; Vasiliev, S.K.; O’Gorman, K.; Derevianko, A.P.; et al. Timing of archaic hominin occupation of Denisova Cave in southern Siberia. *Nature* **2019**, *565*, 594–599. [[CrossRef](#)]
109. Galbraith, R.F.; Roberts, R.G.; Laslett, G.M.; Yoshida, H.; Olley, J.M. Optical dating of single and multiple grains of quartz from jinnium rock shelter, northern Australia, part 1, Experimental design and statistical models. *Archaeometry* **1999**, *41*, 339–364. [[CrossRef](#)]
110. Thomsen, K.J.; Murray, A.S.; Botter-Jensen, L.; Kinahan, J. Determination of burial dose in incompletely bleached fluvial samples using single grains of quartz. *Radiat. Meas.* **2007**, *42*, 370–379. [[CrossRef](#)]
111. Arnold, L.J.; Roberts, R.G.; Galbraith, R.F.; DeLong, S.B. A revised burial dose estimation procedure for optical dating of young and modern-age sediments. *Quat. Geochronol.* **2009**, *4*, 306–325. [[CrossRef](#)]
112. Smedley, R.K. A new R function for the Internal External Uncertainty (IEU) model. *Anc. TL* **2015**, *33*, 16–21.
113. Hu, G.M.; Li, S.H. Simplified procedures for optical dating of young sediments using quartz. *Quat. Geochronol.* **2019**, *49*, 31–38. [[CrossRef](#)]
114. Roberts, R.G.; Galbraith, R.F.; Yoshida, H.; Laslett, G.M.; Olley, J.M. Distinguishing dose populations in sediment mixtures: A test of single-grain optical dating procedures using mixtures of laboratory-dosed quartz. *Radiat. Meas.* **2000**, *32*, 459–465. [[CrossRef](#)]

115. Roberts, R.G.; Flannery, T.F.; Ayliffe, L.K.; Yoshida, H.; Olley, J.M.; Prideaux, G.J.; Laslett, G.M.; Baynes, A.; Smith, M.A.; Jones, R.; et al. New ages for the last Australian megafauna: Continent-wide extinction about 46,000 years ago. *Science* **2001**, *292*, 1888–1892. [[CrossRef](#)]
116. Jacobs, Z.; Duller, G.A.T.; Wintle, A.G.; Henshilwood, C.S. Extending the chronology of deposits at Blombos Cave, South Africa, back to 140 ka using optical dating of single and multiple grains of quartz. *J. Hum. Evol.* **2006**, *51*, 255–273. [[CrossRef](#)]
117. Feathers, J.; Kipnis, R.; Pilo, L.; Arroyo-Kalin, M.; Coblenz, D. How old is Luzia? Luminescence dating and stratigraphic integrity at Lapa Vermelha, Lagoa Santa, Brazil. *Geoarchaeology* **2010**, *25*, 395–436. [[CrossRef](#)]
118. Fu, X.; Cohen, T.J.; Fryirs, K. Single-grain OSL dating of fluvial terraces in the upper Hunter catchment, southeastern Australia. *Quat. Geochronol.* **2019**, *49*, 115–122. [[CrossRef](#)]
119. Lamothe, M.; Auclair, M. A solution to anomalous fading and age shortfalls in optical dating of feldspar minerals. *Earth Planet. Sci. Lett.* **1999**, *171*, 319–323. [[CrossRef](#)]
120. Lamothe, M.; Auclair, M. The fadia method: A new approach in luminescence dating using the analysis of single feldspar grains. *Radiat. Meas.* **2000**, *32*, 433–438. [[CrossRef](#)]
121. Balescu, S.; Lamothe, M.; Auclair, M.; Shilts, W.W. IRSL dating of Middle Pleistocene interglacial sediments from southern Quebec (Canada) using multiple and single grain aliquots. *Quat. Sci. Rev.* **2001**, *20*, 821–824. [[CrossRef](#)]
122. Li, B.; Li, S.H.; Duller, G.A.T.; Wintle, A.G. Infrared stimulated luminescence measurements of single grains of K-rich feldspar for isochron dating. *Quat. Geochronol.* **2011**, *6*, 71–81. [[CrossRef](#)]
123. Neudorf, C.M.; Roberts, R.G.; Jacobs, Z. Sources of overdispersion in a K-rich feldspar sample from north-central India: Insights from De, K content and IRSL age distributions for individual grains. *Radiat. Meas.* **2012**, *47*, 696–702. [[CrossRef](#)]
124. Trauerstein, M.; Lowick, S.; Preusser, F.; Rufer, D.; Schlunegger, F. Exploring fading in single grain feldspar IRSL measurements. *Quat. Geochronol.* **2012**, *10*, 327–333. [[CrossRef](#)]
125. Feathers, J.; Tunnicliffe, J. Effect of single-grain versus multi-grain aliquots in determining age for K-feldspars from southwestern British Columbia. *Anc. TL* **2011**, *29*, 53–58.
126. Reimann, T.; Thomsen, K.J.; Jain, M.; Murray, A.S.; Frechen, M. Single-grain dating of young sediments using the pIRIR signal from feldspar. *Quat. Geochronol.* **2012**, *11*, 28–41. [[CrossRef](#)]
127. Van Gorp, W.; Veldkamp, A.; Temme, A.J.A.M.; Maddy, D.; Demir, T.; van der Schriek, T.; Reimann, T.; Wallinga, J.; Wijbrans, J.; Schoorl, J.M. Fluvial response to Holocene volcanic damming and breaching in the Gediz and Geren rivers, western Turkey. *Geomorphology* **2013**, *201*, 430–448. [[CrossRef](#)]
128. Trauerstein, M.; Lowick, S.E.; Preusser, F.; Schlunegger, F. Small aliquot and single grain IRSL and post-IR IRSL dating of fluvial and alluvial sediments from the Pativilca valley, Peru. *Quat. Geochronol.* **2014**, *22*, 163–174. [[CrossRef](#)]
129. Brown, N.D.; Rhodes, E.J.; Antinao, J.L.; McDonald, E.V. Single-grain post-IR IRSL signals of K-feldspars from alluvial fan deposits in Baja California Sur, Mexico. *Quat. Int.* **2015**, *362*, 132–138. [[CrossRef](#)]
130. Rhodes, E.J. Dating sediments using potassium feldspar single-grain IRSL: Initial methodological considerations. *Quat. Int.* **2015**, *362*, 14–22. [[CrossRef](#)]
131. Gliganic, L.A.; Cohen, T.J.; Meyer, M.; Molenaar, A. Variations in luminescence properties of quartz and feldspar from modern fluvial sediments in three rivers. *Quat. Geochronol.* **2017**, *41*, 70–82. [[CrossRef](#)]
132. Reimann, T.; Roman-Sanchez, A.; Vanwalleghem, T.; Wallinga, J. Getting a grip on soil reworking—Single-grain feldspar luminescence as a novel tool to quantify soil reworking rates. *Quat. Geochronol.* **2017**, *42*, 1–14. [[CrossRef](#)]
133. Brill, D.; Reimann, T.; Wallinga, J.; May, S.M.; Engel, M.; Riedesel, S.; Bruckner, H. Testing the accuracy of feldspar single grains to date late Holocene cyclone and tsunami deposits. *Quat. Geochronol.* **2018**, *48*, 91–103. [[CrossRef](#)]
134. Riedesel, S.; Brill, D.; Roberts, H.M.; Duller, G.A.T.; Garrett, E.; Zander, A.M.; King, G.E.; Tamura, T.; Burow, C.; Cunningham, A.; et al. Single-grain feldspar luminescence chronology of historical extreme wave event deposits recorded in a coastal lowland, Pacific coast of central Japan. *Quat. Geochronol.* **2018**, *45*, 37–49. [[CrossRef](#)]
135. Schaarschmidt, M.; Fu, X.; Li, B.; Marwick, B.; Khaing, K.; Douka, K.; Roberts, R.G. pIRIR and IR-RF dating of archaeological deposits at Badahlin and Gu Myaung Caves—First luminescence ages for Myanmar. *Quat. Geochronol.* **2019**, *49*, 262–270. [[CrossRef](#)]

136. Smedley, R.K.; Buylaert, J.P.; Ujvari, G. Comparing the accuracy and precision of luminescence ages for partially-bleached sediments using single grains of K-feldspar and quartz. *Quat. Geochronol.* **2019**, *53*, 101007. [[CrossRef](#)]
137. Guo, Y.; Li, B.; Zhao, H. Comparison of single-aliquot and single-grain MET-pIRIR De results for potassium feldspar samples from the Nihewan Basin, northern China. *Quat. Geochronol.* **2020**, *56*, 101040. [[CrossRef](#)]



© 2020 by the authors. Licensee MDPI, Basel, Switzerland. This article is an open access article distributed under the terms and conditions of the Creative Commons Attribution (CC BY) license (<http://creativecommons.org/licenses/by/4.0/>).